Polymer 50 (2009) 1743–1754

Contents lists available at ScienceDirect

Polymer

journal homepage: www.elsevier.com/locate/polymer

Nanocomposites formed from polypropylene/EVA blends

C.G. Martins [a], N.M. Larocca [a], D.R. Paul [b], L.A. Pessan [a,*]

[a] Department of Materials Engineering, Universidade Federal de São Carlos, Via Washington Luiz, Km 235, 13565-905, São Carlos SP, Brazil
[b] Department of Chemical Engineering, University of Texas at Austin, Austin, TX 78712, USA

ARTICLE INFO

Article history:
Received 5 December 2008
Received in revised form
27 January 2009
Accepted 29 January 2009
Available online 4 February 2009

Keywords:
Nanocomposites
Polypropylene
Blend

ABSTRACT

Rubber toughened polypropylene nanocomposites using two types of modified montmorillonite (organoclay) were explored with the objective of achieving an improved balance between stiffness and toughness. The effect of three blending sequences on microstructure and properties of the ternary nanocomposites was also investigated. A commercial grade of ethylene/vinyl acetate copolymer (EVA) containing 18 wt% of vinyl acetate was used as the impact modifier for polypropylene and an acrylic acid grafted polypropylene was used to compatibilize the systems studied. The toughened nanocomposites samples were prepared by melt compounding in a twin-screw extruder; the morphology and mechanical properties of the resulting materials were characterized by X-ray scattering, electron microscopy and tensile and impact testing. The results show that incorporation of EVA increases the toughness of the polypropylene but its stiffness decreased markedly due to the incorporation of the low modulus component. The addition of organoclay increased the modulus slightly for all the ternary nanocomposites with respect to the blend, but it remains lower than that of neat PP. Surprisingly, addition of organoclay to the blends promoted a drastic increase in the notched Izod impact strength and a considerable alteration of the shape of the dispersed EVA phase when the organoclay is located in this phase. Moreover, it was found that the blending sequence effects on the morphology and properties of the mixtures are dependent on the organoclay used.

1. Introduction

Blending two or more immiscible polymers can be an effective way to obtain a polymeric system with properties that can be even better than those of the neat polymers or with a useful combination of properties. A good example of the former is the incorporation of elastomeric particles in a glassy matrix to obtain a blend with toughness greater than either neat polymer [1–3]. A more recent technique for modifying polymers is incorporation of organically modified layered silicates to form polymeric nanocomposites. If the individual platelets of these organoclays or aggregates with a small number of platelets are dispersed in the polymer matrix even at low loading level of these silicates (about 5 wt%), the resulting nanocomposites can exhibit remarkable improvement in certain properties compared to the neat polymer, e.g., high modulus and heat distortion resistance [4–6]. More recently, these two approaches for polymer modification have been used together to achieve polymer systems that combine the properties of blends and nanocomposites, for example, high impact strength and modulus [7–12]. However, there is much to be learned about the mechanisms by which the clay platelets influence the morphology and mechanical properties of the blends.

The effect of organoclays on the morphology of blends has been mentioned numerous times in the recent literature. It appears that when the organoclay is located in the continuous phase, there is a reduction of the domain size of the dispersed phase related to a reduction of the coalescence rate of the dispersed phase and/or a compatibilizing effect of the organoclay at the interface between the two phases with perhaps some contribution from the increased melt viscosity of the matrix. Conversely, when the organoclay is located in the dispersed phase, there often appears to be an increase in the dispersed phase domain size [13–19].

As a consequence of the modification of the blend morphology due to the incorporation of organoclay, the mechanical properties are also altered. Some studies have investigated the relationship between the location of the organoclay in blends with elastomeric dispersed particles and the corresponding mechanical properties, such as in the system poly(butylene terephthalate), PBT/maleated ethylene–vinyl acetate copolymer, EVA-*g*-MA/organoclay [7] and Nylon 66/SEBS-*g*-MA/organoclay [8,20]. In these studies, the addition of organoclay to the blend leads to higher stiffness and lower toughness with the best balance achieved when the organoclay platelets are located in the continuous phase instead of in the dispersed phase. On the other hand, other reports show that

* Corresponding author. Tel.: +55 16 33518533; fax: +55 16 33615404.
E-mail address: pessan@ufscar.br (L.A. Pessan).

0032-3861/$ – see front matter © 2009 Elsevier Ltd. All rights reserved.
doi:10.1016/j.polymer.2009.01.059

addition of organoclay to a blend can lead to an increase of the toughness of the ternary nanocomposite relative to the neat blend as found for the system PP/ethylene–octene elastomer blend [9] in addition to the expected increase in modulus. This was attributed to the decrease in the size of the dispersed elastomeric phase that enhances the toughness and compensates at least partially the intrinsic decrease of the toughness by the introduction of the rigid organoclay phase.

Some other papers report an enhancement of the toughness when the clay platelets were located at the interface or in the elastomeric disperse phase. For example, Kelnar et al. [21,22] found that ternary blends of polyamide-6/EPR/organoclay showed increased toughness relative to the neat blend in spite of the lamellar stacks of the clay located around the EPR disperse particles but not in the matrix. Another example is the ternary blend of PP/SBS/organoclay studied by Li et al. [23]. The clay platelets in this system were located in the dispersed SBS phase and the toughness increased with the addition of organoclay to the blend. These apparent contradictory results suggest that the effect of the organoclay on the mechanical properties of ternary blends probably is not limited to a modification of the blend morphology and more studies in other ternary blends would help to better understand the relationship between the clay location and toughness.

In this work, the ternary blend-nanocomposite system PP/EVA/organoclay was investigated in order to gain insights about the correlation between the mechanical properties of this system and its morphology and location of the clay platelets. The motivation for using PP as the matrix in this ternary system is its good processability, chemical resistance and low cost. However, the ability for PP to be used as an engineering thermoplastic is still limited by its poor mechanical properties, in particular toughness (impact resistance) and stiffness (modulus) [24]. Therefore, it is expected that the simultaneous incorporation of an elastomeric phase (EVA) and a rigid phase (organoclay) could lead to an attractive material with simultaneous enhancements in toughness and stiffness relative to the neat PP. Blending sequence (order of organoclay incorporation in the blend) is explored to see its effect on the blend morphology and clay platelets location and, in turn, how these factors affect mechanical properties. These investigations were carried out for two types of organoclays with different polarity of the organic modifier in order to see how this influences the morphology, clay location and dispersion and mechanical properties.

2. Experimental

2.1. Materials

A polypropylene homopolymer with a melt flow index of 3.5 g/10 min (230 °C/16 kg) and trade name of H 501 HC was supplied by Braskem (Brazil). A EVA copolymer with a content of 18% vinyl acetate by weight and a melt flow index of 2 g/10 min (190 °C/16 kg) was supplied as pellets by Triunfo Petrochemical (Brazil) under the trade name of Tritheva® PN 2021. A polypropylene grafted with 6 wt% of acrylic acid with a melt flow index of 40 g/10 min (230 °C/16 kg) from Crompton Chemical (Polybond® 1001) was used as compatibilizer.

The organoclays Cloisite®30B and Cloisite®20A were purchased from Southern Clay Products Inc. Cloisite®30B is a natural montmorillonite with a cation exchange capacity of 90 mequiv/100 g that has been ion exchanged with methyl, tallow, bis-2-hydroxyethyl quaternary ammonium chloride to form an organoclay. The weight loss on ignition of Cloisite®30B was ~30%. Cloisite®20A is also a natural montmorillonite that has been ion exchanged with dimethyl, dehydrogenated tallow, quaternary ammonium chloride to form an organoclay. The weight loss on ignition of Cloisite®20A was ~38%.

Our rationale for choosing these organoclays was as follows. Cloisite®20A is an organoclay with no polar groups on its organic salt while the organic modifier in Cloisite®30B does have polar hydroxyl groups. It was expected that the latter organoclay might have better interaction with the polar EVA than Cloisite®20A, while the opposite trend is expected for PP.

2.2. Nanocomposite preparation

All materials were vacuum dried for at least 12 h prior to melt processing. The ternary nanocomposites were prepared in a twin-screw extruder, B&P Process Equipment Systems, model MP19 ($L/D = 25$, $D = 19$ mm). The temperature profile was 170, 190, 190, 190, 195 °C and the screw speed was set at 140 rpm. The extrudates were pelletized at the die exit, dried and then molded into test specimens using an Arburg 270 V injection-molding machine operated at an injection pressure of 430 bar and a holding pressure of 350 bar. The temperature profile was 190, 200, 215, 225, 225 °C and the mold temperature was held at 40 °C. Izod bars and dogbone bars with dimensions according to ASTM D256-06 and ASTM D638-02a were molded for impact testing and tensile testing, respectively.

In order to study the effect of blending sequence on the morphology and properties of the ternary nanocomposites, three sequences were adopted:

- mixture M1 (PP + PP-*g*-AA + EVA + organoclay): polypropylene, acrylic acid grafted polypropylene, EVA and organoclay were blended simultaneously.
- mixture M2 (PP + PP-*g*-AA + organoclay) + EVA: polypropylene and acrylic acid grafted polypropylene were first reinforced with organoclay and then the polypropylene/acrylic acid grafted polypropylene/organoclay nanocomposite was later blended with EVA.
- mixture M3 PP + PP-*g*-AA + (EVA + organoclay): EVA was mixed with organoclay first and then the EVA/organoclay nanocomposite was blended with polypropylene and acrylic acid grafted polypropylene later.

For all the sequences, the weight% of PP, PP-*g*-AA and EVA was 55, 5 and 40%, respectively. The weight% of organoclay was 5% over the weight of the blend (that is, 5 phr).

Additionally, PP/PP-*g*-AA/organoclay (95/5/5) and EVA/organoclay (100/5) binary nanocomposites and PP/EVA/PP-*g*-AA (55/40/5) binary blend were prepared. The binary and ternary nanocomposites and the blend were prepared under the same compounding conditions described above. The composition of the blend without organoclay was chosen based on a previous report [25]; this composition showed the best balance between stiffness and toughness between all the compositions of the binary blends studied.

The ternary nanocomposites (PP + PP-*g*-AA + EVA+organoclay), (PP + PP-*g*-AA+organoclay) + EVA and PP + PP-*g*-AA + (EVA + organoclay) are designated hereafter as: M1, M2, and M3 respectively. The different types of mixtures with clay are referred to as $M1_{20A}$, $M2_{20A}$, $M3_{20A}$, $M1_{30B}$, $M2_{30B}$ and $M3_{30B}$. For example, $M3_{20A}$ means EVA was mixed with organoclay first and then the EVA/organoclay nanocomposite was blended with polypropylene and acrylic acid grafted polypropylene later; the organoclay used was Cloisite®20A. For the sake of simplicity, PP-*g*-AA is omitted from the designation of PP binary nanocomposites and where organoclay is added to the blends with EVA; thus, the designation PP refers to PP/PP-*g*-AA 95/5.

2.3. Mechanical and thermo-mechanical properties

Tensile tests were conducted on the injection molded specimens according to ASTM D638 using an Instron Model 5569 at a cross-head speed of 50 mm/min. Notched Izod impact tests were performed at room temperature using a Ceast model RESIL 25 pendulum according to ASTM D256.

The thermo-mechanical behavior of the samples was examined using a MK-II Polymer Laboratories dynamic mechanical thermal analyzer (DMTA). The experiments were carried out in bending mode on the injection molded Izod specimens from −50 to 150 °C at a rate of 3 °C/min and at frequency of 1 Hz. The heat distortion temperature (HDT) of the samples was estimated by DMTA using a technique developed by Scobbo [26] and used also by Paul et al. [27,28]. ASTM standard D648 defines the HDT as the temperature at which the center deflection Δ of a standard specimen in a three-point bend mode reaches 0.25 mm under an applied maximum stress σ_{max} of either 0.46 or 1.82 MPa. The condition of 1.82 MPa stress was selected because it is typically employed for semi-crystalline and filled polymers. Utilizing the equation for the center deflection of a simply supported beam we have the relationship between the modulus E, the maximum stress and the deflection [26]:

$$E = \sigma_{max} L^2 / 6\Delta h \quad (1)$$

Where L is the distance between end supports and h is the depth of specimen (equivalent to the width, if the specimen is tested in a edgewise position). By taken into account that $L = 100$ mm and $h = 12.5$ mm (values defined by ASTM standard) and that $\sigma_{max} = 1.82$ MPa and $\Delta = 0.25$ mm, E is approximately 0.75 GPa. Thus, from a DMTA curve of the logarithm of the storage modulus E' vs. temperature, the HDT was determined as the temperature which $E' = 0.75$ GPa or $\log E' = 8.9$.

2.4. Morphology characterization

In order to study the dispersion and location of the organoclays in the PP, EVA and the PP/EVA blends, these samples were examined by transmission electron microscopy (TEM). Ultra-thin sections about 70 nm thick were cryogenically cut from the core of the injection molded Izod specimens in such a way that the sections were perpendicular to the injection flow. The sectioning was done with a diamond knife at a temperature of −110 °C for the EVA specimens with both organoclays used and at a temperature of −55 °C for all other samples using a Leica Ultracut ultramicrotome. After sectioning, the samples were collected on 400 mesh copper TEM grids and dried with filter paper. Sections of the neat blend were stained with RuO_4 vapor for 4 h at room temperature. However, for the blends containing organoclays, it was necessary to increase the temperature to 50 °C during the staining, otherwise these blends could not be stained. From this staining procedure, the EVA phase became darker than the PP phase and, thus, it was possible to determine whether the organoclay platelets were located in the PP phase or in the EVA phase. The sections were viewed using a Philips CM120 transmission electron microscope at an acceleration voltage of 120 kV.

Besides TEM, the PP/EVA blend and PP/EVA/organoclay blends were also examined by scanning electron microscopy (SEM) in order to study the dispersion of the EVA particles in the PP matrix and, therefore, the effect of the clay layers on this dispersion. Surfaces of injection molded samples were cryogenically fractured perpendicular to the injection flow direction and were etched with toluene at 40 °C for 2 h to remove the EVA phase and then observed using a Philips XL30 FEG scanning electron microscope.

2.5. X-ray analysis

Wide angle X-ray scattering (WAXD) was conducted using a Rigaku (Multiflex) diffractomer in the reflection mode using an incident X-ray wavelength of 1.542 Å at a scan rate of 0.5°/min in a range of 2θ from 1 to 10°. The analyses were carried out on milled Izod bars and, therefore, the structure analyzed corresponds to the core of the injection-molded specimens.

3. Results and discussion

3.1. WAXD analysis

3.1.1. WAXD analysis of nanocomposites with Cloisite®20A

Fig. 1a shows X-ray scans of neat Cloisite®20A, the binary systems of EVA and PP with Cloisite®20A and the ternary systems (PP/EVA/Cloisite®20A). For the binary systems it can be seen that the d_{001} peak shifts to the left (lower angles) with respect to the peak of the pristine organoclay suggesting intercalation of the polymer molecules into the galleries of the clay. The d-spacings for the nanocomposites with EVA and PP with compatibilizer (Table 1) are in good agreement with values found in the literature for mixtures with similar compositions and processing [29,30]. The larger d-spacing for the nanocomposite of EVA (3.84 nm) in comparison with the nanocomposite of PP (2.55 nm) suggests greater intercalation of EVA; this may reflect a more favorable interaction of the EVA, in comparison with the PP + PP-*g*-AA system, with the platelets of the organoclay. This speculation is in accord with the results of the work of Cui et al. [29] where it was found that the higher the vinyl acetate content of EVA, the greater the d-spacing for the Cloisite®20A organoclay. The mixtures M1, M2 and M3 with Cloisite®20A show similar d-spacings as the binary nanocomposite EVA/Cloisite®20A, see Fig. 1 and Table 1. This suggests that in these mixtures the organoclay Cloisite®20A tends to reside in the EVA phase, even though the possibility of the presence of exfoliated clay platelets in this phase and in the PP phase cannot be ruled out, since clay in an exfoliated state would result in a featureless WAXD curve.

3.1.2. WAXD analysis of nanocomposites with Cloisite®30B

In contrast with the nanocomposites prepared with Cloisite®20A, Fig. 1b shows that the d_{001} peak shifts to the right (higher angles) for the binary nanocomposites with Cloisite®30B suggesting a decrease of the d-spacing of the galleries of the organoclay. Similar behavior has been reported previously for nanocomposites of organoclay Cloisite®30B with EVA [29–32], with EVA grafted with maleic anhydride groups [33] and with PP [34,35,36]; this has been attributed to the thermal degradation and loss of some parts of the surfactant from the galleries of the organoclay during processing causing collapse of the clay galleries. The phenomena observed here with Cloisite®20A and Cloisite®30B are in agreement with the results of the works done by Paul et al. [29,37,38] who showed that the organic modifier with only one alkyl tail (like Cloisite®30B) is less thermally stable than the organoclay with two alkyl tails (like Cloisite®20A).

Some recent reports on EVA nanocomposites claim better intercalation/exfoliation for the nanocomposites of EVA with Cloisite®30B than with Cloisite®20A [33,39–41]. These studies used milder processing conditions (i.e., temperatures between 100 and 160 °C in an internal mixer) than those used here, this could lead to a lower degree of degradation of the organoclay Cloisite®30B. Under less severe conditions, it is possible that the hydroxyl groups of the organic modifier present in organoclay Cloisite®30B interact with the polar acetate groups of EVA before this degradation takes place. This is in accordance with a report by Li and Ha [33] that

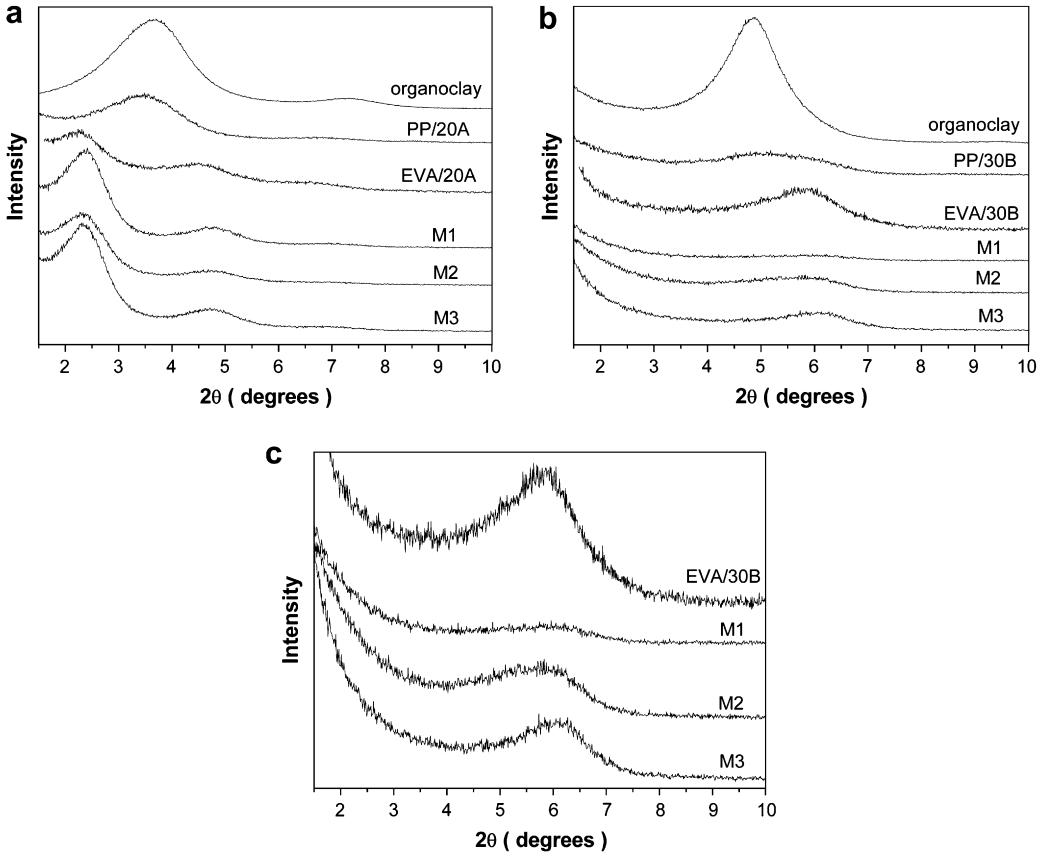

Fig. 1. WAXD scans for neat organoclays, binary nanocomposites (PP/organoclay and EVA/organoclay) and ternary nanocomposites (PP/EVA/organoclay): (a) systems with Cloisite®20A; (b) systems with Cloisite®30B; (c) expanded view of region of part b.

better dispersion of Cloisite®30B in EVA occurs at lower mixing temperatures (130 °C), while at higher temperatures (175 °C) a d_{001} peak is observed at about the same 2θ value found in the present work (6°).

Fig. 1b and Table 1 show that the shift of the d_{001} peak to higher angles for the nanocomposite PP/Cloisite®30B is smaller than the corresponding shift for the nanocomposite EVA/Cloisite®30B. The degradation products released by organoclays are mainly long alkyl fragments [29,42]. Shah and Paul [37] argued that these products can only leave the clay galleries during melt processing by dissolution in the matrix polymer. Thus, if the alkyl fragments have high solubility in the matrix, the organic mass of the galleries is easily extracted and the platelets would then collapse. In the present case, it is not clear whether the by-products of the degradation reaction would be more soluble in EVA (82 wt% ethylene sequences) or in PP. Therefore, it is difficult to predict how this argument would favor gallery collapse in EVA vs. PP.

3.2. TEM analysis

3.2.1. TEM analysis of nanocomposites with Cloisite®20A

TEM micrographs of the binary nanocomposites and ternary nanocomposites based on Cloisite®20 are presented in Figs. 2 and 3, respectively. Fig. 2a–b shows a coarse morphology for the Cloisite®20A in the PP matrix with tactoids of varying sizes; however, there is no evidence of individual platelets dispersed in PP. This is consistent with the WAXD results and with the morphologies found in the literature for similar nanocomposites of PP with PP-*g*-AA and Cloisite®20A [33]. On the other hand, TEM images for EVA/Cloisite®20A nanocomposites, see Fig. 2c, show a significant number of individual platelets dispersed in the EVA phase plus some small tactoids.

For the ternary mixtures M1, M2 and M3, the TEM images reveal the dispersion state of the organoclay, and whether the organoclay resides in the EVA phase or in the PP phase. In these TEM micrographs, see Fig. 3, the darker phase is the EVA phase, since it is stained by the RuO_4. As described earlier, the staining of the blends at room temperature was adequate to promote good phase contrast in the TEM; however, for blends containing organoclays it was necessary to perform a more intense staining at 50 °C. We believe this resistance to staining is due to the decreased RuO_4 permeability into the EVA phase when nanoclay platelets are present; it is well-known that nanocomposites have lower vapor and gas permeability than the neat polymer [43–45].

The images in Fig. 3 seem to indicate that the organoclay resides in the EVA phase for all the ternary mixtures corroborating the WAXD observation; there is no clear evidence of clay platelets in the PP phase. In the EVA phase, there are some exfoliated single platelets in the bulk and at the interface of this phase but small

Table 1
Organoclay interlayer spacing obtained by WAXD.

	d_{001} (Å)	
	Cloisite®20A	Cloisite®30B
Neat organoclay	24.2	18.4
PP/organoclay	25.5	17.2
EVA/organoclay	38.4	15.1
M1	36.9	14.8
M2	38.4	15.8
M3	37.7	14.6

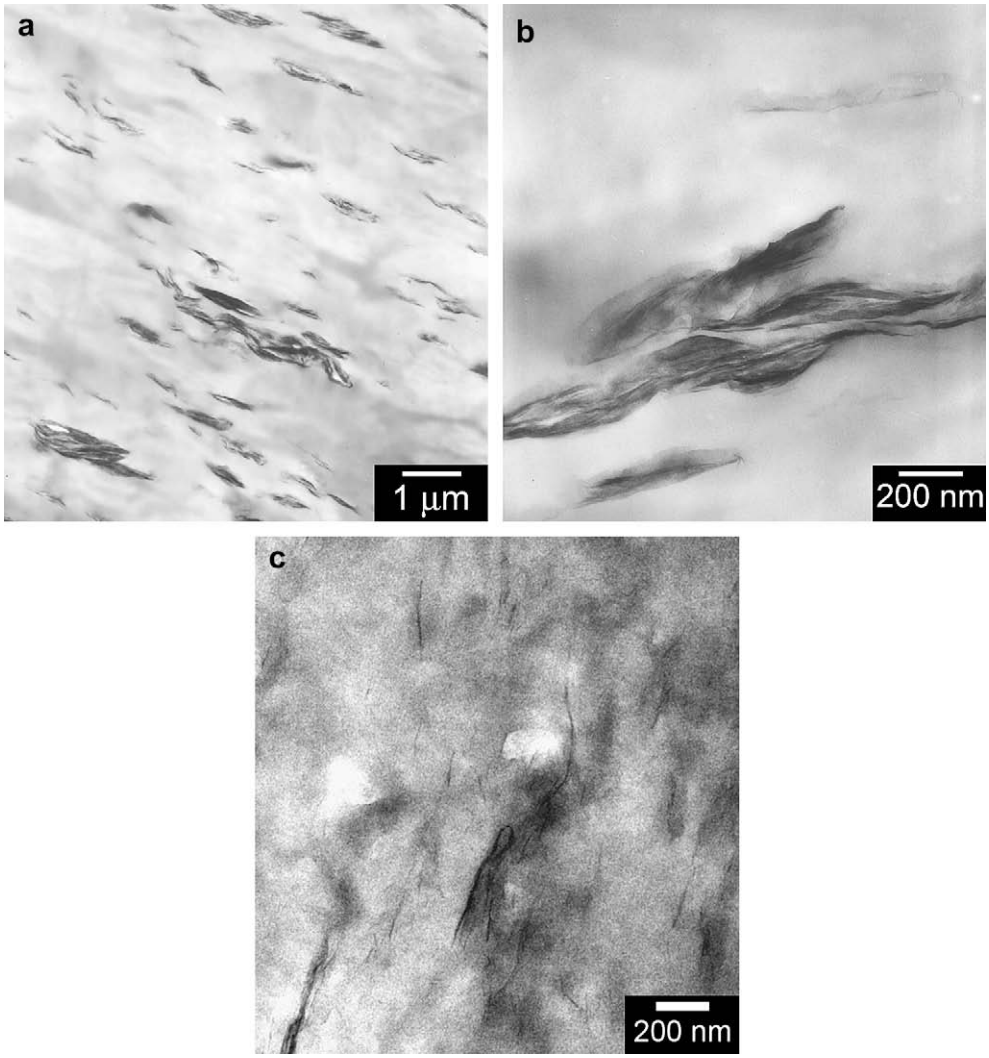

Fig. 2. TEM micrographs of binary nanocomposites with Cloisite®20A: (a) PP/organoclay(8800×); (b) PP/organoclay (40,000×); (c) EVA/organoclay (40,000×).

tactoids account for the majority of the organoclay. This is somewhat different from what is seen for the binary EVA/Cloisite®20A nanocomposites (Fig. 2c), where a larger amount of organoclay is dispersed as individual platelets. However, this difference might be expected because if one assumes that all the organoclay is concentrated in the EVA phase (which represents 40 wt% of the blend), the effective concentration of the organoclay in this phase is around 12 phr vs. 5 phr in the binary nanocomposite. This high concentration of organoclay in the EVA phase favors platelet–platelet interaction and aggregation, leading to the formation of a high content of small tactoids.

In summary, irrespective of the blending sequence, the platelets of the organoclay Cloisite®20A always seem to be located in the EVA phase. The organoclay platelets are attracted to the EVA phase even in the mixture M2, where the organoclay is first blended with PP and the EVA is incorporated subsequently. In this blend sequence apparently all the organoclay initially present in the PP phase migrated to the EVA phase during the short residence time (about 1 min) of the second extrusion. This observation shows that this organoclay definitely has a stronger affinity for EVA than for the PP/PP-*g*-AA mixture and that this migration process is relatively fast. This observation is analogous to the preferential location of methacrylated butadiene-styrene (MBS) particles into the poly (methyl methacrylate) (PMMA) phase in a blend of polycarbonate (PC)/PMMA/MBS [46]. This location occurs irrespective of the blending sequence and can be explained by the more favorable interaction of the MBS particles with PMMA than with PC.

3.2.2. TEM analysis of nanocomposites with Cloisite®30B

Fig. 4 shows TEM micrographs for binary nanocomposites with Cloisite®30B. In the case of PP, small and large tactoids of the organoclay are observed, some having length and width as large as 8 μm and 1 μm, respectively; these are effectively primary organoclay particles that have not been broken up in the compounding process [47]. The tactoids seen in the PP/Cloisite®20A nanocomposites are much smaller and more numerous than seen here for PP/Cloisite®30B. A similar qualitative comparison exists for the binary nanocomposites based on EVA. Fig. 4a shows that in the binary nanocomposite of EVA/Cloisite®30B some exfoliated platelets coexist with tactoids that are much larger than the tactoids present in the binary nanocomposite of EVA/Cloisite®20A (Fig. 2a). A similar feature has also been reported by Zaragoza et al. [31].

The TEM micrographs of the ternary mixtures with Cloisite®30B (Fig. 5) show that the location and dispersion of this organoclay in the blend phases are not the same for all the sequences used to prepare the blends, which is in contrast with the behavior observed for the blends with Cloisite®20A. The mixtures M1 and M2 contain only tactoids, some of which have

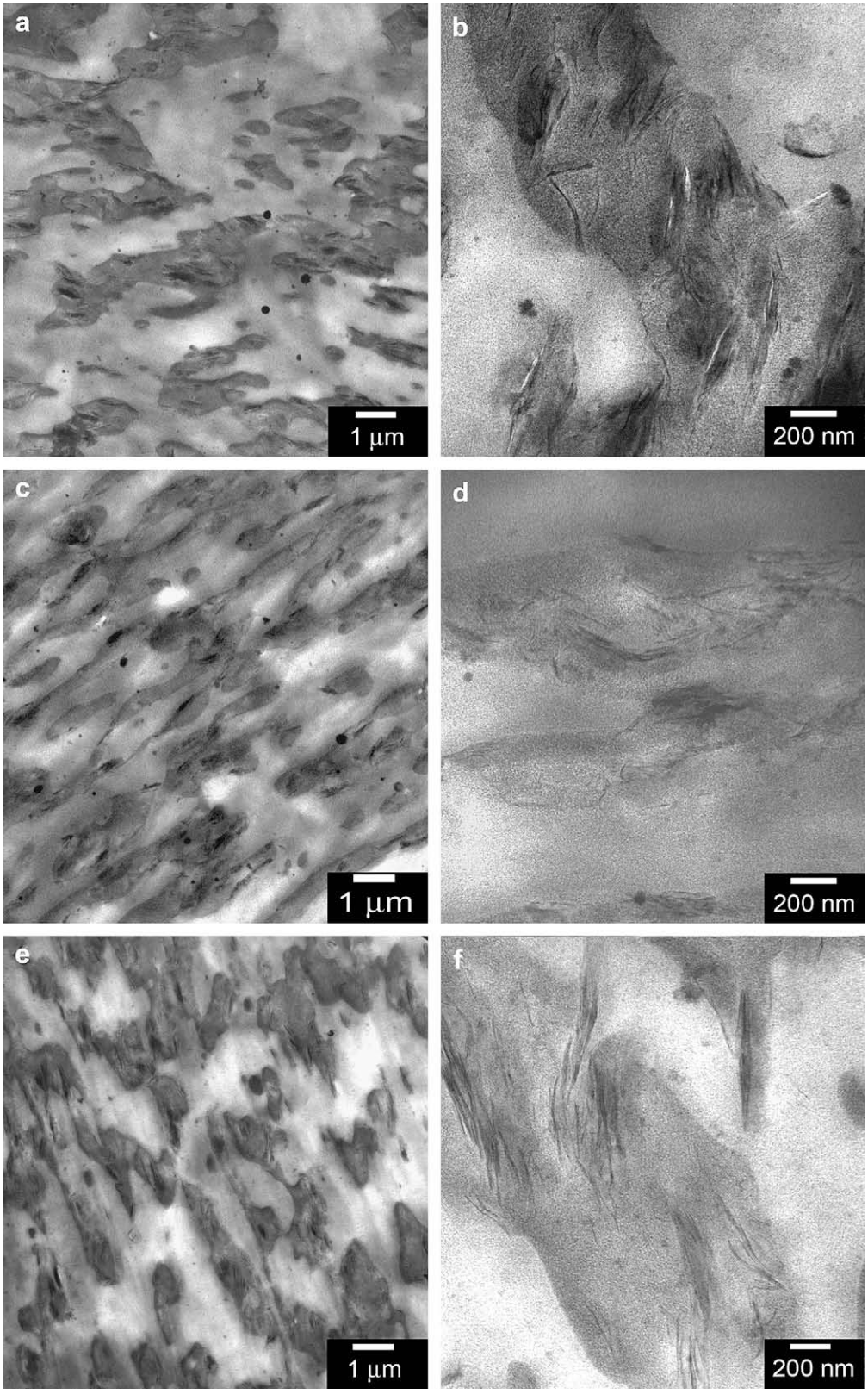

Fig. 3. TEM micrographs of ternary nanocomposites with Cloisite®20A: (a), (c) and (e): micrographs with magnification of 7100× of the mixtures M1, M2 and M3, respectively; (b), (d) and (f): micrographs with magnification of 40,000× of the mixtures M1, M2 and M3, respectively.

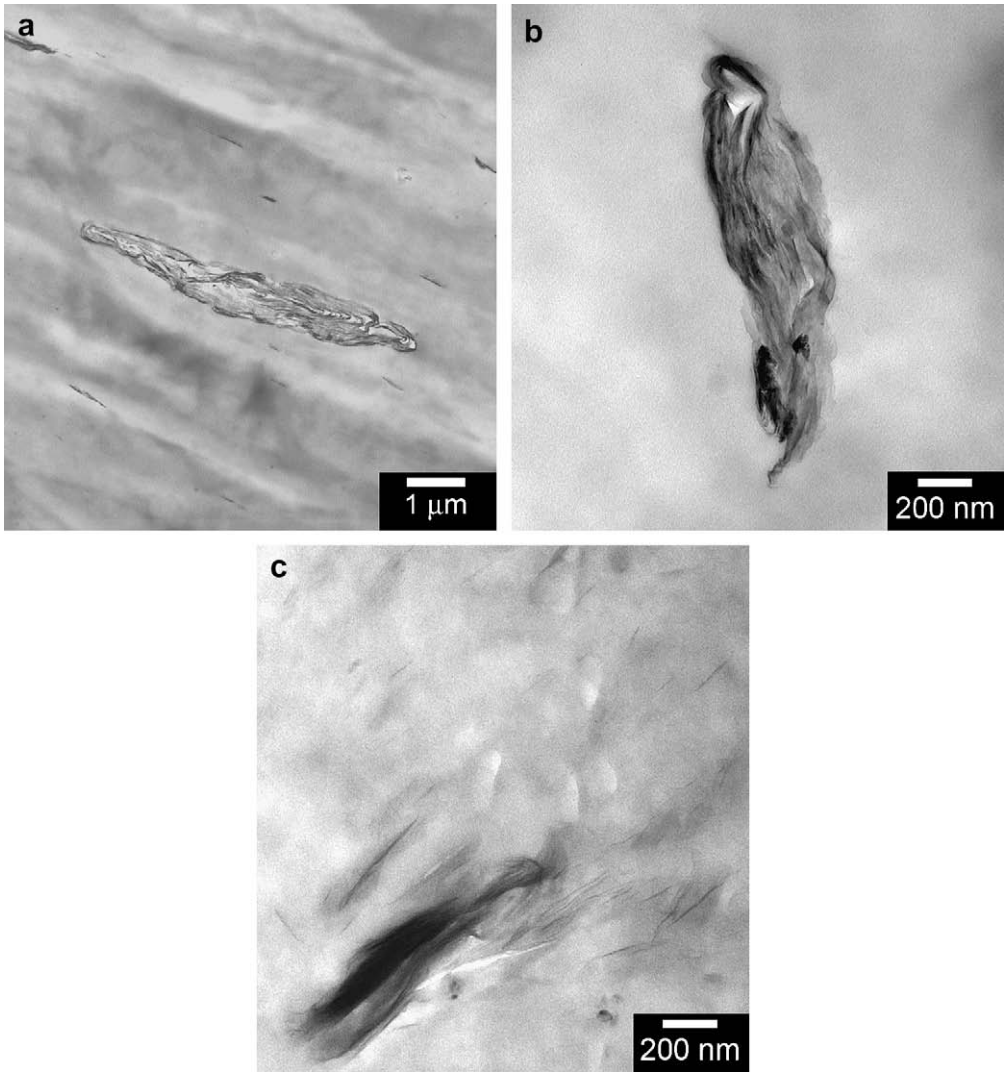

Fig. 4. TEM micrographs of binary nanocomposites with Cloisite®30B: (a) PP/organoclay(8800×); (b) PP/organoclay (40,000×); (c) EVA/organoclay (40,000×).

dimensions as large as those found for the binary nanocomposites, with no evidence of dispersed individual platelets. The majority of these tactoids seem to locate at the interface between the polymer phases. The mixture M3 shows a different picture with apparently all the organoclay dispersed into the EVA phase as a mixture of exfoliated platelets and small tactoids. It is possible that the majority of the tactoids in mixtures M1 and M2 is not located in the EVA phase because the movement of these large particles could be too slow to reach this phase in a local process time-scale comparative with the reciprocal of the processing shear rate (about $10^3\ s^{-1}$). Cheng et al. [46] found that the characteristic time for the movement of a particle across the interface is proportional to the particle radius if only surface forces act to move this particle. Conversely, for the mixture M3, the tactoids are located in the EVA phase because in this mixture the organoclay is forced to be dispersed in this phase prior the mixing with the PP + PP-*g*-AA.

The trend for large tactoids observed here for the binary nanocomposites with Cloisite®30B is consistent with the WAXD results that showed evidence of collapse of the clay galleries for this organoclay. However, it should be pointed out here that exfoliated platelets of this organoclay were still present in the nanocomposite EVA/Cloisite®30B.

The morphology of the binary nanocomposites reflects a complex interplay of shear forces during melt mixing where the main role of the shear is to break down the initial clay agglomerates into progressively smaller tactoids [48–51], the peeling away of platelets from the tactoids when there is sufficient affinity of the platelets for the polymer matrix, and the possible competing effects of degradation of the surfactant that complicates these processes. The situation in ternary mixtures is even more complex.

3.3. Scanning electron microscopy: blend morphology

SEM analysis was used to ascertain the phase morphology of the ternary nanocomposites over a larger area than was observed by TEM and specifically to examine the spatial arrangement of the EVA and PP phases. The SEM photomicrographs of the neat blend (without organoclay) and ternary nanocomposites are depicted in Figs. 6 and 7, respectively. Comparison of the morphology of the ternary nanocomposites of PP/EVA/Cloisite®20A (Fig. 7 a–c) with the neat blend (Fig. 6), reveals that in these nanocomposites the shape of the EVA particles is irregular, with smaller curvature and larger anisotropy than the particles in the neat blend. For the ternary nanocomposites of PP/EVA/Cloisite®30B (Fig. 7 d–f), this irregular morphology occurs for the mixture M3, but not for the

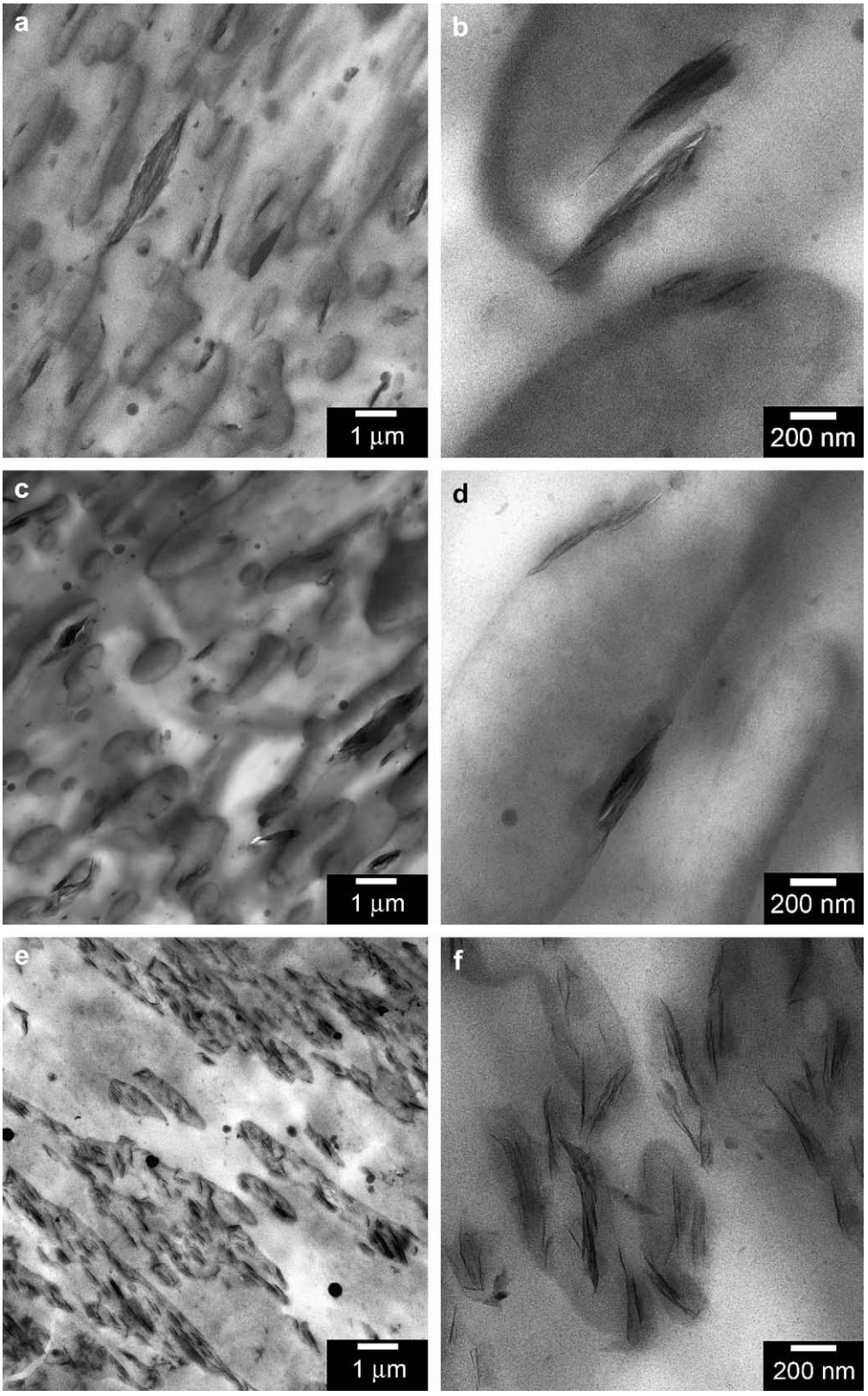

Fig. 5. TEM micrographs of ternary nanocomposites with Cloisite®30B: (a), (c) and (e): micrographs with magnification of 7100× of the mixtures M1, M2 and M3, respectively; (b), (d) and (f): micrographs with magnification of 40,000× of the mixtures M1, M2 and M3, respectively.

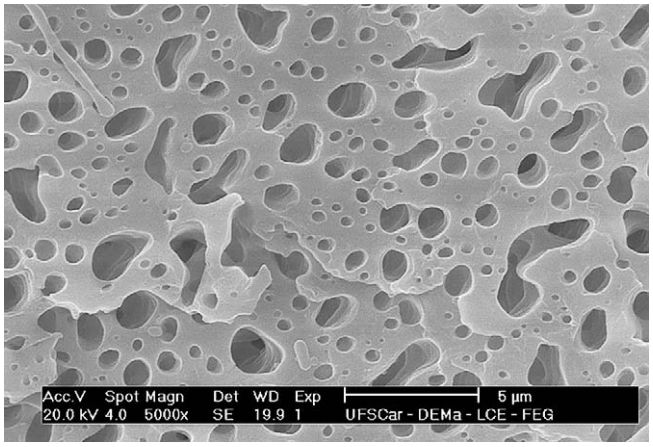

Fig. 6. SEM micrograph of neat PP/PP-*g*-AA/EVA blend.

mixtures M1 and M2; the latter have a morphology very similar to the neat blend. The EVA particles in the ternary nanocomposites seem to have an average size comparable to that of neat blend. However, a quantitative analysis of the particle sizes for the ternary nanocomposites was not practical due to the anisotropy and irregularity of the EVA particles in these mixtures.

From the TEM and the SEM photomicrographs, a clear correlation between the clay location and the morphology of the EVA particles, irrespective of the organoclay can be seen; that is, the EVA particles are anisotropic when the organoclay is located inside the particles. It is likely that this shape is due to the presence of a fraction of exfoliated clay particles located at the interface PP/EVA. We speculate that the presence of clay platelets at the interface between PP and EVA lead to the irregular shape of the EVA particles by hindering the rounding promoted by the interfacial tension in the neat PP/EVA blend. Similar lamellar shapes of the disperse phase have also been found in other blends when the organoclay is located in the disperse phase, like in the blends EPR/PP [15], PMMA/PS [16], PP/PA6 [17,18] and PE/PBT [19].

3.4. Mechanical and thermo-mechanical properties

Table 2 shows values for the tensile modulus, yield stress, notched Izod impact strength and HDT for the neat polymers, binary blends and the ternary mixtures. As mentioned earlier, the HDT was estimated using the storage modulus curves (Fig. 8) obtained from DMTA analysis. Estimates of HDT values, defined at a maximum stress of 1.82 MPa, correspond to the temperature where the E' curve crosses the horizontal line drawn at this stress on the log E' axis (line illustrated in the plots of Fig. 8).

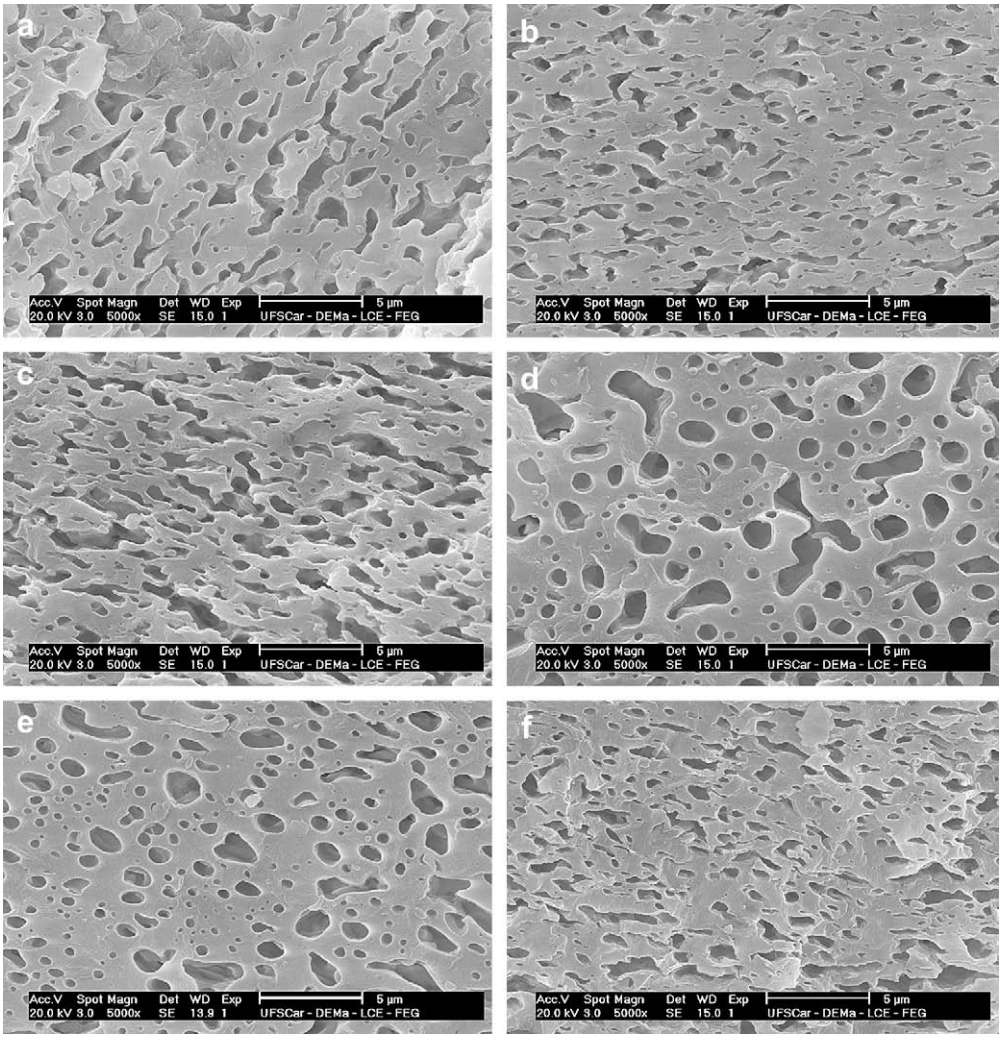

Fig. 7. SEM micrographs of ternary nanocomposites: with Cloisite®20A: mixtures M1(a) M2 (b) and M3 (c). With Cloisite®30B: mixtures M1(d) M2 (e) and M3 (f).

Table 2
Mechanical and thermo-mechanical properties of the neat polymers and nanocomposites.

Composition	Tensile modulus (GPa)	Yield strength (MPa)	Heat distortion temperature (°C)	Izod impact strength (J/m)
PP	2.17 ± 0.13	38.0 ± 0.1	57	19 ± 2
PP_{20A}	2.58 ± 0.13	41.5 ± 0.4	66	22 ± 3
PP_{30B}	2.34 ± 0.06	39.1 ± 0.2	61	23 ± 2
EVA_{20A}	–	–	−12	–
EVA_{30B}	–	–	−15	–
PP/EVA18/PP-g-AA (55/40/5)	1.05 ± 0.18	22.3 ± 0.3	24	124 ± 3
$M1_{20A}$	1.27 ± 0.12	22.8 ± 0.5	33	244 ± 18
$M2_{20A}$	1.24 ± 0.14	22.6 ± 0.2	31	252 ± 16
$M3_{20A}$	1.16 ± 0.06	22.6 ± 0.3	33	217 ± 23
$M1_{30B}$	1.22 ± 0.03	23.1 ± 0.3	29	87 ± 2
$M2_{30B}$	1.36 ± 0.18	24 ± 1	27	84 ± 4
$M3_{30B}$	1.18 ± 0.10	22.6 ± 0.2	30	195 ± 7

As seen in Table 2, the binary nanocomposites based on PP show increased modulus, yield stress and HDT compared to PP, while the Izod impact strength is essentially unchanged considering the standard deviation associated with this measurement. Prior work suggests that the extent of enhancement of the modulus as well as HDT are indicators of the aspect ratio of the organoclay particles dispersed in the polymer matrix and, therefore, reflect the state of exfoliation or dispersion of the organoclay [27,52]. Thus, it is seen that the increase of modulus is more significant for the nanocomposite based on Cloisite®20A than on Cloisite®30B; the same trend is observed for the yield stress and HDT, consistent with the presence of smaller primary particles in the nanocomposites of the former organoclay than the latter one as shown by TEM analysis. Similar correlations can be seen between the organoclay morphologies and the properties of the binary nanocomposites of EVA. It should be mentioned that the relative efficacy of the organoclay Cloisite®20A in comparison with Cloisite®30B in improving the mechanical properties may be even greater than the results shown here. This is because the comparison shown here is at a fixed content of organoclay, i.e., 5 wt%, thus, the effective concentration of inorganic alumina–silicate platelets is lower for the nanocomposites based on Cloisite®20A than Cloisite®30B, since the organic content of the former organoclay is higher than for the latter, 38 vs. 30 wt%, respectively.

From Table 2 it can be seen also that the incorporation of 40 wt% of EVA in PP decreases the modulus, yield stress and HDT but increases the Izod impact strength; that is, there is a decrease of stiffness and an increase of toughness caused by incorporation of this elastomeric phase. Addition of organoclays to the PP/EVA blend leads to a slight increase in modulus and HDT, and a marginal increase in yield stress; these changes are nearly independent of the organoclay used and of the blending sequence, considering the standard deviations of the measurements. Overall, the average increase in modulus and HDT is 18% and 25%, respectively; however, despite this increase, the values for the mixtures with nanoclays are still significantly below those for the neat PP.

The notched Izod impact strength of the mixtures with organoclays show more interesting but complex trends. Compared to the neat blend, there is a significant increase in Izod values for all the mixtures with the Cloisite®20A; the increase is about 100% for mixtures M1 and M2 and 75% for mixture M3. For the mixtures with Cloisite®30B, toughness is increased only for mixture M3 (increase of 57%), while there is a decrease in the toughness for the mixtures M1 and M2.

The changes in stiffness and toughness can be best appreciated by plotting the tensile modulus vs. Izod impact strength (Fig. 9) and the HDT against Izod impact strength (Fig. 10). From these figures, it is clear that, for all the mixtures with Cloisite®20A and for the mixture M3 with Cloisite®30B, the organoclays are more effective for improving impact strength than for reinforcement; the opposite effect was found for binary nanocomposites of PP.

There is a close correlation between the morphology of the mixtures and their mechanical properties. The incorporation of organoclays into PP/EVA blends leads to only a slight improvement in modulus and HDT. This is probably due to the small concentration of clay in the PP continuous phase; for all mixtures with Cloisite®20A and the mixture $M3_{30B}$, the clay is located primarily in the EVA phase and in the case of the mixtures $M1_{30B}$ and $M2_{30B}$ the large clay tactoids are located mainly at the EVA/PP interface. Prior studies have shown that the enhancement of stiffness is small when the clay is located in the dispersed phase or at the interface instead of in the matrix polymer [7,17,18,22,23,53].

There is also a clear connection between the toughness of these systems and their morphology. The mixtures $M1_{30B}$ and $M2_{30B}$, both of which have a lower Izod impact strength than the neat blend, contain large tactoids of Cloisite®30B. Most likely these large organoclay particles act as stress concentrators that lead to easy crack initiation and propagation and, thus, premature failure with low energy absorption.

On the other hand, all the other mixtures showed an enhancement of the Izod impact strength relative to the neat blend, and in these cases the organoclay is rather well dispersed/exfoliated inside the EVA dispersed phase. This is consistent with several others reports on blends with organoclays showing an increase in toughness when the organoclay is exclusively located in the

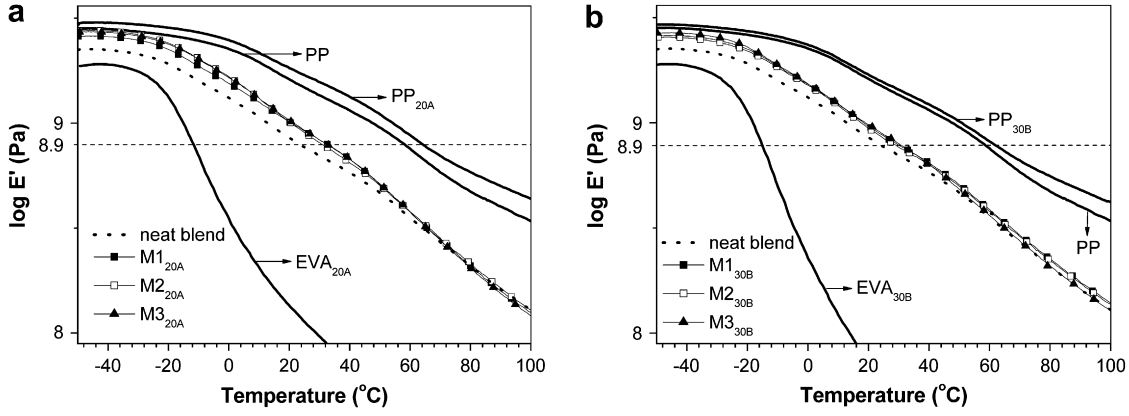

Fig. 8. DMTA curves of storage modulus (E') vs. temperature for the systems studied: (a) systems with Cloisite®20A; (b) systems with Cloisite®30B.

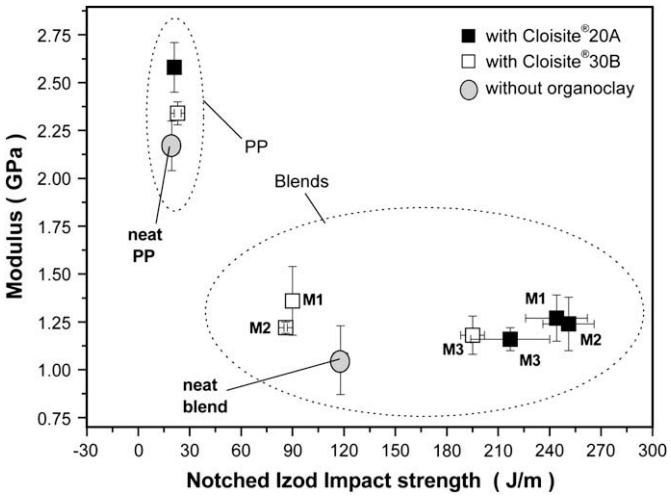

Fig. 9. Plots of tensile modulus vs. notched Izod impact strength for the systems studied.

dispersed phase or at the interphase between the two polymers [21,23,53]. It is anticipated that the toughness of the neat blends is related, at least to some extent, to the cavitation of EVA particles; this is a well-known aspect of toughening mechanism in polymer blends [1,2]. The incorporation of clay platelets in these particles may advantageously control the cavitation process and the stress at which shear yielding of the matrix occurs, thus enhancing blend toughness. Another possibility is related to the mechanism of toughening proposed by Gersappe [54]. According to this theory, the clay platelets could create temporary cross-links between the EVA chains, thereby increasing the strength of the polymer in the vicinity of the micro-voids originated by the cavitation process. This could decrease the growth rate of these micro-voids and therefore increase the dissipation of energy.

On the basis of these results and the discussion above, it can be postulated that dispersing the organoclay in both the EVA and PP phases would lead to greater improvement in stiffness while maintaining high toughness. In this situation, the organoclay in the EVA would promote toughness while having the organoclay in the matrix would increase stiffness. This could be achieved by increasing the polarity of the matrix since this would promote a higher affinity of the matrix for the organoclay. This increase of polarity could be obtained, for example, by increasing the concentration of the functional PP-*g*-AA mixed in the PP matrix. The use of another compatibilizer, like PP grafted with maleic anhydride (PP-*g*-MA) also might be an effective strategy. These approaches are currently being investigated in our laboratory.

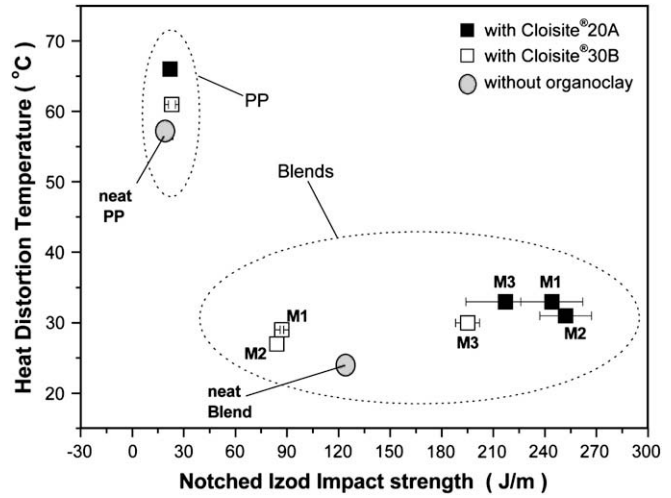

Fig. 10. Plots of heat distortion temperature (HDT) vs. notched Izod impact strength for the systems studied.

4. Conclusions

In this work, ternary nanocomposites of PP/EVA/organoclay in the weight ratio 60/40/5 were prepared by three different blending procedures. In all cases, the phase labeled PP contained 91.7% PP homopolymer and 8.3% of an acrylic acid graft, i.e., PP-*g*-AA, with the latter acting as a "compatibilizer". The influence of blending sequence on the dispersion and location of the organoclay in the blends is dependent on the kind of organoclay used. For Cloisite®20A where the organic modifier has two long alkyl groups, the organoclay is always located in the dispersed EVA phase, irrespective of the blending sequence adopted. However, for Cloisite®30B where the organic modifier is polar and has only one long alkyl group, the organoclay is located in the dispersed EVA phase only when this organoclay is first mixed with EVA. There is a clear relationship between the clay location and the morphology in the ternary nanocomposites, as well as between the morphology and the mechanical properties of these systems. For the blends where the organoclay is in the dispersed EVA phase, the particles of this phase have a lamellar shape, and the impact strength is considerably higher than for the neat blend. On the other hand, for the ternary nanocomposites where the platelets are not well dispersed in the EVA phase, the impact strength is decreased relative to the neat blend. The modulus and HDT, however, are nearly independent of the type of organoclay. The blends with the highest impact strength are those containing Cloisite®20A in which case mixing protocol has only a minor effect. An important result of this work is the observation that Cloisite®20A can migrate from the PP phase to the EVA phase at a surprisingly high rate.

Acknowledgments

The authors would like to thank the Conselho Nacional de desenvolvimento Científico e Tecnológico, CNPq for financial support.

References

[1] Bucknall CB. Deformation mechanisms in rubber-toughened polymers. In: Paul DR, Bucknall CB, editors. Polymer blends, vol. 2. New York: Wiley; 2000. p. 83–117 [chapter 22].
[2] Corte L, Leibler L. Macromolecules 2007;40(15):5606–11.
[3] Larocca NM, Hage Jr E, Pessan LA. Polymer 2004;45(15):5265–77.
[4] Pinnavaia TJ, Beall GW. Polymer–clay nanocomposites. New York: John Wiley & Sons; 2000.
[5] Ray SS, Okamoto M. Prog Polym Sci 2003;28(11):1539–641.
[6] Paul DR, Robeson LM. Polymer 2008;49(15):3187–204.
[7] Li XC, Park HM, Lee JO, Ha CS. Polym Eng Sci 2002;42(11):2156–64.
[8] Dasari A, Yu ZZ, Mai YW. Polymer 2005;46(16):5986–91.
[9] Lee HS, Fasulo PD, Rodgers WR, Paul DR. Polymer 2005;46(25):11673–89.
[10] Gonzalez I, Eguiazabal JI, Nazabal J. Eur Polym J 2006;42:2905–13.
[11] Ahn YC, Paul DR. Polymer 2006;47:2830–8.
[12] Ke Wang, Wang C, Li J, Su J, Qin Zhang, Du R, et al. Polymer 2007;48:2144–54.
[13] Khatua BB, Lee DJ, Kim HY, Kim JK. Macromolecules 2004;37(7):2454–9.
[14] Ray SS, Pouliot S, Bousmina M, Utracki LA. Polymer 2004;45(25):8403–13.
[15] Kontopoulou M, Liu YQ, Austin JR, Parent JS. Polymer 2007;48(15):4520–8.
[16] Si M, Araki T, Ade H, Kilcoyne ALD, Fisher R, Sokolov JC, et al. Macromolecules 2006;39(14):4793–801.
[17] Gahleitner M, Kretzschmar B, Van Vliet G, Devaux J, Pospiech D, Bernreitner K, et al. Rheol Acta 2006;45(4):322–30.
[18] Gahleitner M, Kretzschmar B, Pospiech D, Ingolic E, Reichelt N, Bernreitner K. J Appl Polym Sci 2006;100(1):283–91.
[19] Hong JS, Han Namkung, Ahn KH, Lee SJ, Kim C. Polymer 2006;47(11):3967–75.

[20] Dasari A, Yu ZZ, Yang MS, Zhang QX, Xie XL, Mai YW. Compos Sci Technol 2006;66(16):3097–114.
[21] Kelnar I, Kotek J, Kapralkova L, Hromadkova J, Kratochvil J. J Appl Polym Sci 2006;100(2):1571–6.
[22] Kelnar I, Khunova V, Kotek J, Kapralkova L. Polymer 2007;48(18):5332–9.
[23] Li YM, Wei GX, Sue HJ. J Mater Sci 2002;37(12):2447–59.
[24] Karger-Kocsis J, editor. Polypropylene; structure, blends and composites. Cambridge: Chapman & Hall; 1995.
[25] Martins CG, Larocca NM, Pessan LA, in preparation.
[26] Scobbo JJ. Thermomechanical performance of polymer blends. In: Paul DR, Bucknall CB, editors. Polymer blends, vol. 2. New York: Wiley; 2000. p. 335–57 [chapter 29].
[27] Fornes TD, Paul DR. Polymer 2003;44(17):4993–5013.
[28] Laura DM, Keskkula H, Barlow JW, Paul DR. Polymer 2002;43(17):4673–87.
[29] Cui L, Ma XY, Paul DR. Polymer 2007;48(21):6325–39.
[30] Chinellato AC, Vidotti SE, Hu GH, Pessan LA. J Polym Sci Part B Polym Phys 2008;46(17):1811–9.
[31] Valera-Zaragoza M, Ramırez-Vargas E, Medellın-Rodrıguez FJ. J Appl Polym Sci 2008;108(3):1986–94.
[32] Duquesne S, Jama C, Le Bras M, Delobel R, Recourt P, Gloaguen JM. Compos Sci Technol 2003;63(8):1141–8.
[33] Li XC, Ha CS. J Appl Polym Sci 2003;87(12):1901–9.
[34] Lee JW, Lim YT, Park OO. Polym Bull 2000;45(2):191–8.
[35] Perrin-Sarazin F, Ton-That MT, Bureau MN, Denault J. Polymer 2005;46(25):11624–34.
[36] Lopez-Quintanilla ML, Sanchez-Valdes S, de Valle LFR, Medellin-Rodriguez FJ. J Appl Polym Sci 2006;100(6):4748–56.
[37] Shah RK, Paul DR. Polymer 2006;47(11):4075–84.
[38] Cui L, Khramov DM, Bielawski CW, Hunter DL, Yoon PJ, Paul DR. Polymer 2008;49(17):3751–61.
[39] Peeterbroeck S, Alexandre M, Jerome R, Dubois Ph. Polym Degrad Stab 2005;90(2):288–94.
[40] Chaudhary DS, Prasad R, Gupta RK, Bhattacharya SN. Polym Eng Sci 2005;45(7):889–97.
[41] Chaudhary DS, Prasad R, Gupta RK, Bhattacharya SN. Thermochim Acta 2005;433(1–2):187–95.
[42] Xie W, Gao ZM, Pan WP, Hunter D, Singh A, Vaia R. Chem Mater 2001;13(9):2979–90.
[43] Lape NK, Nuxoll EE, Cussler EL. J Membr Sci 2004;236(1):29–37.
[44] DeRocher JP, Gettelfinger BT, Wang JS, Nuxoll EE, Cussler EL. J Membr Sci 2005;254(1-2):21–30.
[45] Dumont MJ, Reyna-Valencia A, Emond JP, Bousmina MJ. Appl Polym Sci 2007;103(1):618–25.
[46] Cheng TW, Keskkula H, Paul DR. Polymer 1992;33(8):1606–19.
[47] Vaia RA, Jandt KD, Kramer EJ, Giannelis EP. Macromolecules 1995;28(24):8080–5.
[48] Dennis HR, Hunter DL, Chang D, Kim S, White JL, Cho JW, et al. Polymer 2001;42(23):9513–22.
[49] Kim SW, Jo WH, Lee MS, Ko MB, Jho JY. Polym J 2002;34(3):103–11.
[50] Wang K, Liang S, Du RN, Zhang Q, Fu Q. Polymer 2004;45(23):7953–60.
[51] Hommingа D, Goderis B, Hoffman S, Reynaers H, Groeninckx G. Polymer 2005;46(23):9941–54.
[52] Wang J, Pyrz R. Compos Sci Technol 2004;64(7–8):925–34.
[53] Balakrishnan S, Start PR, Raghavan D, Hudson SD. Polymer 2005;46(25):11255–62.
[54] Gersappe D. Phys Rev Lett 2002;89(5):058301-1–058301-4.